Temperature-dependent band structure of $Hg_{1-x}Zn_xTe$-CdTe superlattices

J. Manassès, Y. Guldner, J. P. Vieren, and M. Voos
Laboratoire de Physique de la Matière Condensée, Département de Physique de l'Ecole Normale Supérieure, 24 rue Lhomond, 75005 Paris, France

J. P. Faurie
University of Illinois, Chicago, Illinois 60680
(Received 25 March 1991)

We present transport and far-infrared magneto-optical measurements in narrow-band-gap *n*-type $Hg_{1-x}Zn_xTe$-CdTe superlattices. Hall and conductivity data obtained over a broad temperature range (1.5–300 K) show that these superlattices are semimetallic at low temperature and are degenerate intrinsic semiconductors for $T > 100$ K, which constitutes an interesting situation in semiconductor-superlattice physics. The analysis of the data gives the Fermi energy as well as the temperature-dependent band gap, in good agreement with the calculated band structure, which predicts a semimetal-semiconductor transition induced by temperature in these heterostructures. We have measured the electron cyclotron resonances as a function of temperature with the magnetic field **B** applied parallel and perpendicular to the growth axis. The observed magneto-optical intraband transitions are in very satisfactory agreement with the calculated Landau levels and the Fermi energy. We show that the semimetal-semiconductor transition is characterized by an important reduction of the cyclotron mass measured with **B** perpendicular to the superlattice growth axis. The large variation of the conduction-band anisotropy calculated near the transition accounts for this effect.

I. INTRODUCTION

Considerable progress has been made recently toward the understanding of the complex electronic properties of the so-called type-III superlattices (SL's). These heterostructures, which consist of alternating zero-band-gap and wide-band gap semiconductor layers, can exhibit a positive or a negative energy gap at the Γ point,[1] depending on the layer thicknesses and on temperature. Extensive transport and magneto-optical investigations were reported in HgTe-CdTe and $Hg_{1-x}Zn_xTe$-CdTe superlattices.[2–7] For instance, the zero-temperature band gap has been measured from the temperature dependence of the intrinsic carrier concentration in *p*-type HgTe-CdTe superlattices.[6] The conduction-band dispersion (in particular the band anisotropy) was determined from cyclotron resonance experiments in *n*-type $Hg_{1-x}Zn_xTe$-CdTe SL's,[4] and interband and intraband magneto-optical transitions occurring in the infrared energy range have been observed and interpreted in HgTe-CdTe SL's.[7] The band-structure calculations using a large valence-band offset (300–400 meV) between HgTe and CdTe account for most of these data, in particular for the extremely high electron and hole mobilities observed in the narrow-band-gap SL's.[2]

We report here transport and far-infrared magneto-optical measurements performed over a broad temperature range (1.5–300 K) in three high-quality $Hg_{1-x}Zn_xTe$-CdTe SL's with $x < 0.1$. These type-III heterostructures were grown by molecular-beam epitaxy at the University of Illinois at Chicago and are *n* type with high electron mobilities. Hall and conductivity data obtained as a function of the temperature show that these SL's are degenerate intrinsic semiconductors over a broad temperature range. This constitutes an interesting situation as compared to the transport measurements previously reported in *p*-type HgTe-CdTe SL's,[6] where the valence band was nondegenerate in the intrinsic regime. From the theoretical analysis of these data, the Fermi energy as well as the Γ point gap are obtained as a function of temperature. The SL band-structure calculations, using the envelope function model and a valence-band offset of 360 meV between $Hg_{1-x}Zn_xTe$ ($x < 0.1$) and CdTe, account qualitatively and quantitatively for the observed data. We also report far-infrared magneto-transmission measurements performed on the same SL's in the temperature range 1.5–300 K, with the magnetic field parallel and perpendicular to the growth axis. Intraband and interband transitions are observed in the far-infrared photon energy range in these very-narrow-band-gap SL's. Considering the Fermi energy deduced from the transport measurements, the data are found to agree quite satisfactorily with Landau-level calculations. When the magnetic field is applied perpendicularly to the growth axis, a significant drop is observed in the curve giving the cyclotron mass as a function of the temperature. This drop is associated with the important variation of the conduction-band anisotropy occurring when the SL undergoes a semimetal-semiconductor transition, i.e., when the gap at the Γ point undergoes a sign reversal. The variation of the cyclotron mass and the temperature of the semimetal-semiconductor transition are found to be in good agreement with the band-structure calculations.

II. BAND STRUCTURE AND FERMI LEVEL

A. Description of the samples

We have studied three SL's grown on (100) GaAs substrate with a 2-μm CdTe buffer layer[9] and consisting of 100 periods of $Hg_{1-x}Zn_xTe$-CdTe. The CdTe layers contain approximately 15% HgTe (Ref. 10) since the entire superlattice is grown with the Hg source shutter open in the molecular-beam epitaxy system. For each sample, the layer thicknesses, the alloy Zn composition x as well as the electron mobility and concentration at 25 K are listed in Table I. The SL's are n type in the temperature range investigated in this work (1.5–300 K) with electron mobilities in excess of 2×10^5 cm^2/V s at low temperature. Such high carrier mobilities are usually measured in type-III SL's with a small positive or negative gap at the Γ point.[2,8] Previous magneto-optical experiments[4] reported in similar heterostructures at 1.5 K have shown that they are semimetallic (i.e., the energy gap at the Γ point is negative) at this temperature, and that the valence-band offset between CdTe and low-Zn-content $Hg_{1-x}Zn_xTe$ alloys is large (300–400 meV).

B. Band-structure calculations

We have calculated the SL band structure by using the six-band envelope function model, taking into account the Γ_6 and Γ_8 band edges, which has been described in detail elsewhere.[11] The band parameters of CdTe are taken in Refs. 11 and 12. For $Hg_{1-x}Zn_xTe$ alloys, the temperature variation of the Γ_6-Γ_8 energy separation is given (in meV) by

$$E^{\Gamma_6\text{-}\Gamma_8}(x,T)=-303+2525x+\frac{0.63}{11+T}T^2(1-2x)\ . \quad (1)$$

In Eq. (1), we have assumed[14] $E^{\Gamma_6\text{-}\Gamma_8}=0$ for $x=0.12$ at $T=0$ K. The temperature dependence of $E^{\Gamma_6\text{-}\Gamma_8}$ is chosen identical to that established in HgCdTe alloys close to HgTe.[15] This seems to be justified for $Hg_{1-x}Zn_xTe$ alloys with low Zn content. Figure 1 shows calculated dispersion relations for S_1 in the plane of the layers (k_x) and along the growth axis (k_z) for $T=120$ K [Fig. 1(a)] and $T=1.5$ K [Fig. 1(b)]. The energy origin is taken at the CdTe valence-band edge and the valence-band offset is 360 meV. $E1$ (HH1) denotes the first electron (heavy-hole) band considering the dispersion along k_z. For $T=120$ K, $E1$ is the conduction band, HH1 is the highest valence band, and the Γ-point energy gap $\varepsilon^{S_1}=E_{E1}-E_{HH1}$ is positive (31 meV). The in-plane electron and hole masses near $k_x=0$ are very small

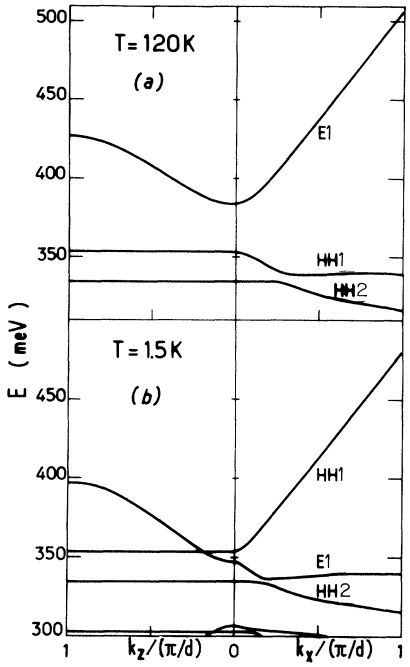

FIG. 1. Calculated band structure of S_1 using $\Lambda=360$ meV in the plane of the layers (k_x) and along the growth axis (k_z) for (a) $T=120$ K and (b) $T=1.5$ K. $d=d_1+d_2$ is the superlattice period.

($<10^{-2}m_0$) and nearly proportional to ε^{S_1} as far as ε^{S_1} is small.[1] $E1$ is light along k_z, so that the conduction band is nearly isotropic around $k=0$ and its density of states is weak. On the contrary HH1 is almost dispersionless along k_z and is extremely nonparabolic in the plane of the layers. As a consequence, when the temperature increases and the hole and electron thermal distribution spreads over a few meV into the HH1 and $E1$ bands, it is clear that the average HH1 density of states is much larger than that for $E1$. This particular feature is observed in all the narrow-band-gap type-III SL's where the HH1 mass along k_x is found to increase dramatically with increasing k_x. This explains, for instance, why the hole mobility decreases strongly[6] when the temperature is raised in p-type superlattices, while a similar mobility drop is not observed for electrons.

When the temperature is decreased, ε^{S_1} is reduced until $E1$ and HH1 meet for $T=30$ K and then cross in the k_z direction for $k_z=k_c$, leading to ε^{S_1} negative. For instance, Fig. 1(b) shows the calculated band structure for

TABLE I. Characteristics of the $Hg_{1-x}Zn_xTe$-CdTe superlattices used in this work. d_1 and d_2 are the $Hg_{1-x}Zn_xTe$ and the CdTe layer thicknesses, respectively, x is the Zn composition; n and μ are measured at 25 K.

Sample	d_1 (Å)	d_2 (Å)	x	μ (cm^2/V s)	n (cm^{-3})
S_1	105	20	0.053	2.1×10^5	3.7×10^{15}
S_2	80	12	0.053	2.1×10^5	2.6×10^{15}
S_3	160	20	0.070	2.4×10^5	2.4×10^{15}

$T=1.5$ K. ε^{S_1} is negative (-6.5 meV) and HH1 displays an electron in-plane dispersion while $E1$ has a hole in-plane dispersion. There is, in fact, a very small anticrossing between HH1 and $E1$ at k_c resulting from k linear terms that we do not take into account in our model. In our analysis, we have neglected the vanishing energy gap which opens up at k_c, so that the band structure of Fig. 1(b) is considered as "semimetallic." The conduction band in the semimetallic regime is dispersionless for $0<k_z<k_c$ and is therefore strongly anisotropic, the in-plane mass being light as a result of the small HH1-$E1$ separation. The valence band is again extremely nonparabolic. Finally, from band structures calculated using expression (1), ε^{S_1} is found to vary linearly for $T>50$ K with a positive temperature coefficient $\alpha=0.35$ meV/K. A somewhat nonlinear and lower variation is obtained at low temperatures. Quite similar results are obtained for S_2 and S_3 where ε^{S_2} and ε^{S_3} are negative at 1.5 K ($\varepsilon^{S_2}=-15.5$ meV, $\varepsilon^{S_3}=-13.5$ meV) and become positive for $T>50$ K.

C. Determination of the Fermi energy and SL band gap

Low magnetic-field ($B<1$ T) transport measurements (Hall effect and conductivity) give the carrier density n and the electron mobility as a function of the temperature in the range 10–300 K. The density n is found to be nearly independent of T at low temperature, from which the donor concentration may be obtained. This leads to $N_D-N_A\approx 3\times 10^{15}$ cm^{-3} in S_1, $N_D-N_A\approx 2\times 10^{15}$ cm^{-3} in S_2 and S_3. Figure 2(a) shows the carrier density n normalized by $T^{3/2}$ as a function of the inverse temperature for S_1 and S_3. It is clear that the condition $n\gg N_D-N_A$ is fulfilled for $T>100$ K so that the SL's are intrinsic over a broad temperature range (100–300 K) as it can be expected in very-narrow-band-gap semiconductors with a low doping level. It is well known that in the intrinsic regime the temperature dependence $n(T)$ can be used to determine the zero-temperature extrapolation of the SL gap. Such measurements were reported successfully in p-type HgTe-CdTe SL's assuming parabolic bands[6] and have given results in satisfactory agreement with the gaps determined from magneto-optical and optical measurements when the comparison was possible. Here the determination of the band gap from the intrinsic carrier density is a little more intricate because our SL's are degenerate intrinsic semiconductors in the temperature range 100–300 K and the usual law of mass action used in Refs. 5 and 6 does not apply to our case. Indeed, it is clear in Fig. 2(a) that the variation $nT^{-3/2}$ plotted on a logarithmic scale versus T^{-1} is not a straight line in the entire intrinsic regime as expected for a nondegenerate semiconductor, but only in the restricted range 200–300 K. From the cyclotron mass measurements as a function of the temperature described in Sec. III, the in-plane dispersion as well as the k_z dispersion of the conduction band are known and, as a consequence, the conduction-band density of states is known too. A first-order estimation of the Fermi energy E_F measured from the bottom of the conduction band is given for each temperature by the

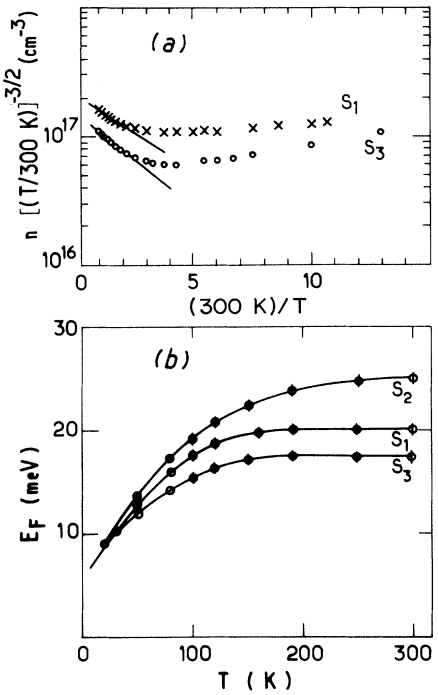

FIG. 2. (a) Experimental carrier density normalized by $T^{3/2}$ vs inverse temperature for S_1 and S_3. The solid lines shows the linear variation between 200 and 300 K as explained in the text. (b) Fermi energy E_F vs temperature for samples S_1, S_2, and S_3 (open dots). Solid lines are only guides for the eye.

expression[16]

$$n(T)=2\left[\frac{kT}{2\pi\hbar^2}m_c^{\mathrm{DOS}}\right]^{3/2}\mathcal{F}_{1/2}(E_F/kT)\ . \tag{2}$$

Here $\mathcal{F}_{1/2}(X)$ is the Fermi-Dirac integral and the density-of-states conduction mass is taken to be $m_c^{\mathrm{DOS}}=m_x^{2/3}m_z^{1/3}$, where the in-plane mass m_x and the mass m_z along k_z are obtained from the cyclotron resonance data. The variation $E_F(T)$ obtained from this analysis is shown in Fig. 2(b) for S_1, S_2, and S_3. Note that E_F is positive in the entire temperature range, which corresponds to a degenerate situation, and that it is nearly constant between 200 and 300 K. The degenerate intrinsic regime arises from the extremely high density of states of the valence band previously discussed. If one assumes an average density-of-states mass m_v^{DOS} for the valence band, a ratio $m_v^{\mathrm{DOS}}/m_c^{\mathrm{DOS}}\approx 30$ is obtained for S_1 in the temperature range 100–300 K by using the expression[16]

$$n(T)=p(T)=2\left[\frac{kT}{2\pi\hbar^2}m_v^{\mathrm{DOS}}\right]^{3/2}\exp\left[\frac{-(E_F+\varepsilon^{S_1})}{kT}\right], \tag{3}$$

where the valence band is assumed to remain nondegenerate. Quite similar high ratios $m_v^{\mathrm{DOS}}/m_c^{\mathrm{DOS}}$ are obtained in S_2 and S_3. Considering that m_c^{DOS}

$\approx 2\times 10^{-2} m_0$ in S_1 for $T=200$ K, one deduces $(m_c^{\mathrm{DOS}} m_v^{\mathrm{DOS}})^{1/2} \approx 0.11 m_0$, in very good agreement with the average value $0.12 m_0$ reported by Hoffman *et al.*[6] in nondegenerate *p*-type HgTe-CdTe SL's in the intrinsic regime. This agreement is not surprising because all the narrow-band-gap type-III SL's have very similar band structures and therefore display similar electronic properties.

Assuming a linear temperature variation of the gap $\varepsilon^{S_1} = \varepsilon_0^{S_1} + \alpha T$, expression (3) can be written in the intrinsic regime:

$$n(T) = 2\left[\frac{kT}{2\pi\hbar^2} m_v^{\mathrm{DOS}}\right]^{3/2} \exp\left[\frac{-\alpha}{k}\right] \exp\left[\frac{-(E_F+\varepsilon_0^{S_1})}{kT}\right]. \tag{4}$$

The Fermi energy level being constant between 200 and 300 K [$E_F \approx 20$ meV; see Fig. 2(b)], a linear variation of $\ln(nT^{-3/2})$ with reciprocal temperature is expected in this temperature region. The slope of the solid line drawn for S_1 in Fig. 2(a) gives directly $E_F + \varepsilon_0^{S_1} \approx 9$ meV and therefore $\varepsilon_0^{S_1} \approx -11$ meV. A similar analysis done in S_2 and S_3 gives the zero-temperature extrapolation of the gap $\varepsilon_0^{S_2} \approx -10$ meV and $\varepsilon_0^{S_3} \approx -8$ meV. These results are in satisfactory agreement with the semimetallic band structure calculated at low temperature using a valence-band offset of 360 meV [see Fig. 1(b)].

Note that it is possible to obtain a more or less accurate determination of the temperature coefficient α from the variation $E_F(T)$ shown in Fig. 2(b) and the cyclotron mass $m_c \approx m_x$ measured at high temperatures. In first approximation, the conduction mass at the energy E_F in a narrow-band-gap semiconductor is given by[1]

$$m_x = m_x^0\left[1+\frac{E_F}{\varepsilon^{S_1}}\right], \tag{5}$$

where the mass m_x^0 at $k_x=0$ is proportional to ε^{S_1}. Assuming that the cyclotron mass is measured at the Fermi energy, one obtains in S_1, $m_x \approx 10^{-2} m_0$ and $m_x \approx 1.8\times 10^{-2} m_0$ at 100 and 200 K, respectively [see Fig. 4(a)]. From expression (5), one deduces immediately $\varepsilon^{S_1}(200\ \mathrm{K}) + E_F(200\ \mathrm{K}) = 1.8\ [\varepsilon^{S_1}(100\ \mathrm{K}) + E_F(100\ \mathrm{K})]$, which leads to $\alpha \approx 0.35$ meV/K, in good agreement with the calculated band-gap variation for $T>50$ K using expression (1) for the Γ_6-Γ_8 separation in $Hg_{1-x}Zn_xTe$ alloys.

Infrared transmission experiments were carried out in S_1, S_2, and S_3 between 400 and 2000 cm^{-1} at 300 K in order to determine the SL band gap. An absorption edge is measured in S_1 for photon energy around 120 meV, in good agreement with the calculated value $\varepsilon^{S_1} + E_F = 115$ meV for 300 K, which corresponds approximately to the fundamental absorption in a degenerate semiconductor. A similar agreement is obtained in S_2 and S_3.

III. MAGNETOTRANSMISSION MEASUREMENTS

We now discuss the far-infrared magnetotransmission experiments performed on samples S_1, S_2, and S_3 using a molecular gas laser ($\lambda = 41-255$ μm) in the temperature range 1.5–300 K. The transmission signal was measured at fixed infrared photon energy, while the magnetic field B could be varied up to 12 T.[17] The measurements were carried out in both the Faraday geometry (with **B** parallel to the growth axis *z*) and the Voigt geometry (with **B** perpendicular to the *z* axis), the propagation wave vector of the incident electromagnetic wave being always parallel to the SL growth axis. Note that in the Faraday geometry, the radiation was not circularly polarized, so that both σ^+ and σ^- polarizations were present.

Typical transmission spectra obtained on S_1 at $\lambda = 118$ μm are shown in Fig. 3 for several temperatures in the Faraday geometry ($\theta = 0°$) and in the Voigt geometry ($\theta = 90°$), where θ is the angle between the SL axis and the applied magnetic field. For $\theta = 0°$, two well-developed resonance minima appear at low temperature for small magnetic field ($B < 1$ T) and shift towards higher B when the temperature is raised. The lower field minimum vanishes progressively and for $T > 60$ K, only the higher field minimum is still observed. Experiments performed in the photon energy range 5–30 meV show that these two minima correspond to magneto-optical transitions whose energy extrapolates to zero at $B=0$. They are therefore attributed to intraband transitions between conduction Landau levels,[4] taking into account the *n*-type nature of the SL and the position of the Fermi level. For the highest photon energies used in these experiments ($E > 20$ meV), additional transmission minima are observed which correspond to interband transitions occurring in this narrow band-gap SL. At $\theta = 90°$, two

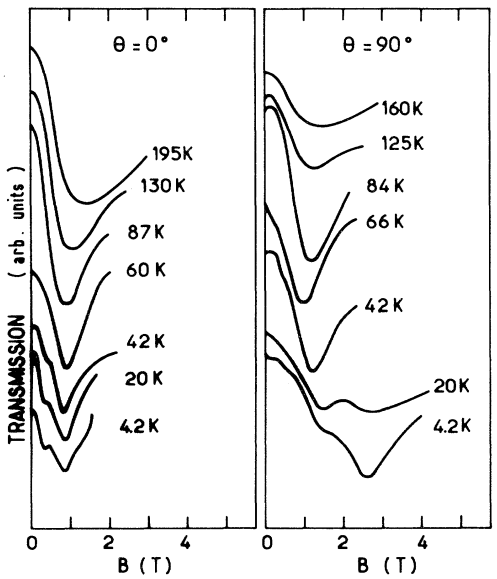

FIG. 3. Transmission spectra obtained on S_1 at $\lambda = 118$ μm for several temperatures in the Faraday ($\theta = 0°$) and Voigt ($\theta = 90°$) geometries.

resonance transmission minima are also observed in Fig. 3 for low temperatures, the higher field line vanishing around 30 K. The low field transition is found to extrapolate to $E=0$ at $B=0$ and is thus attributed to the electron cyclotron resonance. The second line corresponds to a transition with a negative energy extrapolation at $B=0$ and could be associated to an interband transition in this negative band-gap SL for $T<30$ K. It is clear on Fig. 3 that for $\theta=90°$, the first minimum shifts towards low B when T is raised up to 60 K and then moves towards high B for a further temperature increase. As it will be discussed later, this behavior corresponds to the semimetal-semiconductor transition occurring around 30 K in S_1. Moreover, the resonance magnetic field of the first minimum shows a large variation between $\theta=0°$ and 90° at $T=4.2$ K (see Fig. 3). This effect, discussed in a previous paper,[4] corresponds to the large anisotropy of the conduction band and demonstrates the semimetallic band structure of S_1 at low temperature. Quite similar results were obtained in samples S_2 and S_3, which are also semimetallic at low T. A "cyclotron mass" m_c is deduced for each intraband transition from the data by using the simple relation $m_c=eB/\omega$, where ω is the laser pulsation and B the resonance field. The cyclotron masses measured in S_1 at $\lambda=118$ μm are plotted (dots) in Fig. 4 as a function of the temperature in the range 1.5–200 K for $\theta=0°$ [Fig. 4(a)] and $\theta=90°$ [Fig. 4(b)]. Similar results obtained in S_2 are shown in Fig. 5.

In order to interpret the data at $\theta=0°$, the SL Landau-

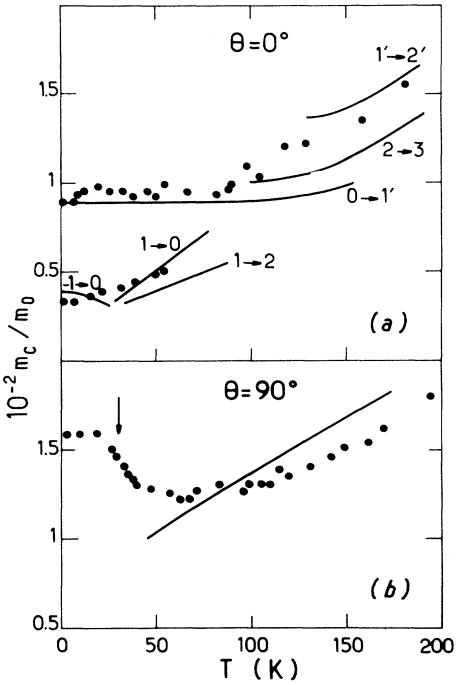

FIG. 4. Cyclotron masses corresponding to the different transmission minima observed in S_1 at $\lambda=118$ μm in the (a) Faraday and (b) Voigt geometries (dots). The solid lines are the theoretical masses calculated from the Landau-level energies at $\theta=0°$ and from the band structure at $\theta=90°$ as described in the text.

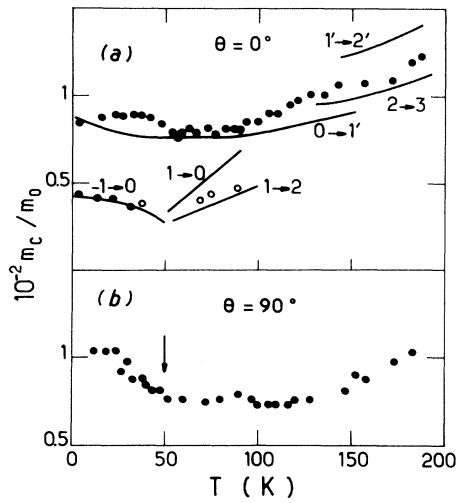

FIG. 5. Cyclotron masses corresponding to the different transmission minima observed in S_2 at $\lambda=118$ μm in the (a) Faraday and (b) Voigt geometries (strong transmission minima, solid dots; weak minima, open dots). The solid lines are the theoretical masses calculated from the Landau-level energies at $\theta=0°$.

level energies are calculated at $k_z=0$ as a function of the temperature by using the six-band envelope function model[11,13] and $\Lambda=360$ meV. Calculations are formally the same as those done at $B=0$ with the Γ_6-Γ_8 energy in $Hg_{1-x}Zn_xTe$ given by expression (1). Figure 6 illustrates the calculated Landau levels of S_1 at $T=1.5$ K [Fig. 6(b)] and 150 K [Fig. 6(a)]. The selection rules for intraband and interband transitions in the Faraday geometry are $\Delta n=\pm1$, where n is the Landau-level index. The transitions actually observed in the SL's depend on the Landau-level occupation and, for this reason, the Fermi-level energy deduced from the transport measurements at vanishing magnetic field is indicated by the dashed line in Fig. 6. We have neglected the oscillations of E_F as a function of the magnetic field. The thermal broadening of width kT on both sides of E_F is shown by the shaded

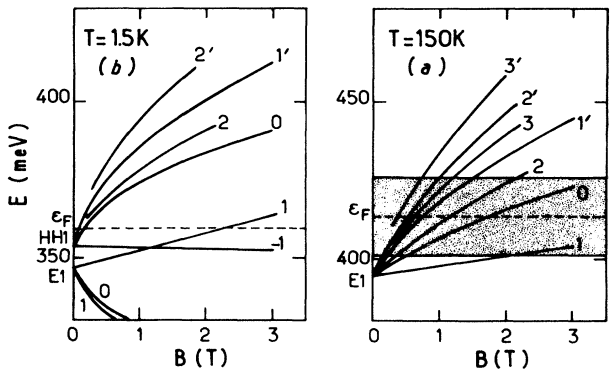

FIG. 6. Calculated Landau-level energies at $k_z=0$ in S_1 using $\Lambda=360$ meV in the (a) semiconducting and (b) semimetallic configuration. The dashed line is the Fermi level and the shaded area represents the thermal broadening kT on both sides of E_F.

region. We have also calculated the Landau-level energies as a function of k_z for given magnetic fields. The width of the conduction Landau levels along k_z is found to be large (>40 meV), except for $n=-1$, which is flat. This arises from the very thin CdTe barriers in these SL's. As a consequence, the transitions observed at $\lambda=118$ μm can only occur at $k_z=0$ and not at the Brillouin-zone boundary. Indeed, at $k_z=\pi/d$, the conduction Landau levels $n\neq 1$ are unoccupied and the energy of the transition $-1\rightarrow 0$ is too large. The solid lines in Figs. 4(a) and 5(a) are the calculated cyclotron masses deduced from the theoretical energy of the intraband transitions. In these calculations, we have taken into account, for each temperature, the initial and final Landau-level occupations, except for the $0\rightarrow 1'$ transition at low temperature, and in Figs. 4(a) and 5(a), the solid lines are limited to the temperature domain where the corresponding transitions can occur. At low temperature, the two resonances correspond to the $-1\rightarrow 0$ and $0\rightarrow 1'$ transitions, which are the two first intraband transitions available in the semimetallic configuration [Fig. 6(b)]. The observation of the $0\rightarrow 1'$ transition is rather puzzling, the Landau level $n=0$ being unoccupied for $B>0.4$ T [Fig. 6(b)]. It is tentatively explained by the existence of an electron accumulation layer at the interface between the SL and the CdTe buffer layer. Such an electron accumulation would result from charge transfer from CdTe towards the SL and was previously observed in [100]-oriented HgCdTe-CdTe heterojunctions,[18] in [100] $Hg_{1-x}Zn_xTe$-CdTe SL's[4] and in [211] HgTe-CdTe SL's.[19] As a consequence, the Fermi level would lie deeper into the conduction band near this interface where a higher cyclotron resonance (for instance $0\rightarrow 1'$) can occur. The electron density of this accumulation layer was found to be approximately equal to 10^{11} cm^{-2} in HgCdTe-CdTe heterojunctions[18] grown in similar conditions to our SL's. Such a density accounts for the magnetotransmission spectra at low temperature in S_1. Note that an electron accumulation could also exist at the front SL surface and give similar results. In the intermediate temperature range 30–60 K for S_1 and 50–90 K for S_2, the SL's are semiconducting and the lower field transition are attributed [Figs. 4(a) and 5(a)] to either $1\rightarrow 2$ or $1\rightarrow 0$, transitions which are both allowed in the Faraday geometry. Considering the variation $E_F(T)$ given in Fig. 2(b) and the thermal broadening kT, the final levels 0 and 2 are more and more occupied when the temperature is raised in this intermediate range. The associated transmission minimum becomes weaker and weaker as T is increased (see Fig. 3) and finally vanishes when $E_F(T)$ is far above the $n=2$ level at the resonant magnetic field (for $T>60$ K in S_1 and $T>90$ K for S_2). In this intermediate-temperature regime, the higher field transition corresponds to $0\rightarrow 1'$. This is consistent with E_F lying between 0 and $1'$ around $B=1$ T. Finally in the high-temperature domain ($T>100$ K), the thermal energy kT becomes comparable to or larger than the photon energy and a single transmission minimum is observed (Fig. 3) which corresponds to the mixing of different intraband transitions. As it is shown in Figs. 4(a) and 5(a), the main transitions observed as T is increased are successively $0\rightarrow 1'$, $2\rightarrow 3$, and $1'\rightarrow 2'$. For instance, it is clear on Fig. 6(a) that at $T=150$ K, $n=1'$ is fully occupied at the resonant field $B=1.2$ T, i.e., its energy lies in the shaded area. The observed transitions at $T=150$ K are therefore $1'\rightarrow 2'$ and $2\rightarrow 3$, as shown in Fig. 4(a). The overall agreement between the magneto-optical data and the calculations is quite satisfying in the entire temperature region investigated in these experiments and supports the calculated Landau levels and band structures using $\Lambda=360$ meV, with a semimetal-semiconductor transition occurring at 30 K in S_1 and 50 K in S_2.

In the Voigt configuration ($\theta=90°$), the most striking feature observed in the dependence $m_c(T)$ on Figs. 4(b) and 5(b) is the drop of approximately 25% appearing around 30 K in S_1 and 40 K in S_2. The cyclotron resonance field is $B\approx 1$ T at $\lambda=118$ μm (Fig. 3) and the cyclotron orbit radius is then larger or comparable to the SL period. The electrons are therefore forced to tunnel through the interfaces for $\theta=90°$ and the cyclotron mass depends on conduction dispersion relations along both k_x and k_z. As the in-plane dispersion shows no dramatic temperature dependence, the important m_c drops must correspond to a significant reduction of the conduction mass m_z along k_z when the temperature varies from 1.5 to 40 K. These observations are in very good agreement with the calculated band structures with $\Lambda=360$ meV (Fig. 1), which show a large variation of the conduction-band anisotropy when the SL undergoes a semimetal-semiconductor transition. Indeed, when the temperature is raised from 1.5 K, the crossing point between $E1$ and HH1 at $k_z=k_c$ moves towards $k_z=0$ and the conduction band becomes lighter and lighter along k_z. The calculated temperatures of the semimetal-semiconductor transition ($k_c=0$) are indicated by the arrows on Figs. 4(b) and 5(b) and are in satisfactory agreement with observed data. Furthermore, it is well known that cyclotron resonance in the Voigt geometry does not usually occur at $\omega_c=eB/m_c$ but rather follows the behavior $\omega=(\omega_c^2+\omega_p^2)^{1/2}$, where ω_p is the plasma frequency. We have carefully investigated the cyclotron resonance in the photon energy range 5–30 meV. A zero-energy extrapolation at $B=0$ for the cyclotron resonance is observed in the temperature region 1.5–60 K and no plasma shift is observed, so that $\hbar\omega_p<5$ meV in this temperature domain. Even if an exact expression of ω_p in a semimetallic or a extremely narrow-band-gap type-III SL is unknown, the condition $\hbar\omega_p<5$ meV seems to be consistent for $T<60$ K with the classical expression given ω_p, if one takes into account the electron density, the SL dielectric constant approximately equal to 20, and the calculated masses m_x and m_z. Moreover, we have checked that the temperature at which the drop occurs in the variation $m_c(T)$ does not depend on the photon energy, as this would be observed in the case of a plasma shifted cyclotron resonance. We are therefore sure that the reduction of m_c observed in Figs. 4(b) and 5(b) is not due to a plasma effect. For $T>50$ K, a monotonic increase of $m_c(T)$ is observed at $\theta=90°$, which corresponds essentially to the opening of the SL band gap when the temperature is

raised, and, as a consequence, to the increase of the in-plane mass. We have not calculated the Landau level energies at $\theta=90°$ and in order to interpret the dependence $m_c(T)$ in the semiconducting configuration ($T>50$ K), we have used the following approximate dispersion relation for the conduction band which takes into account the band nonparabolicity:

$$E(k)=\frac{\Delta E_{E1}}{2}[1-\cos(k_z d)]+\frac{\hbar^2(k_x^2+k_y^2)}{2m_0(1+E/\varepsilon^S)} . \quad (6)$$

Here ΔE_{E1} is the width of the conduction band along k_z which is 45, 110, and 35 meV for S_1, S_2, and S_3, respectively, at $T=120$ K; ε^S is the SL band gap determined in Sec. II; and the origin $E=0$ is taken at the bottom of the conduction band. In a semiclassical approach, the cyclotron mass is simply given by[20,21]

$$m_c=\frac{\hbar^2}{2\pi}\left[\frac{dA}{dE}\right]_{E=E_F} , \quad (7)$$

where A is the extremal area of the section perpendicular to B of the constant energy surface $E=E_F$. The solid line in Fig. 4(b) shows the variation $m_c(T)$ obtained for S_1 in the semiconducting regime from this simple model. In these calculations, we have used the dependence $E_F(T)$ given in Fig. 2(b). The agreement with the experimental data is satisfying, if one takes into account the crude approximation made in this model. For a more detailed analysis of these results, calculations of the Landau levels at $\theta=90°$ would be necessary. Note in Fig. 5 that for high temperatures the S_2 cyclotron mass at $\theta=90°$ is lighter than at $\theta=0°$. As far as we know, this constitutes the first observation of a conduction mass-anisotropy ratio m_z/m_x less than unity in a SL and arises from the extremely thin CdTe barriers (12 Å) in S_2.

IV. CONCLUSION

We have discussed transport and far-infrared magneto-transmission measurements performed in three n-type $Hg_{1-x}Zn_xTe$-CdTe SL's over a broad temperature range. The temperature-dependent electron concentration together with the conduction-band density of states deduced from cyclotron resonance data show unambiguously that these SL's are degenerate in the entire temperature region and are degenerate intrinsic semiconductors for $T>100$ K, which constitutes an interesting situation in semiconductor superlattice physics. The analysis of the data gives the Fermi energy, the negative band gap of the SL's at $T=0$ as well as the temperature coefficient of the band gap. Band structures calculated using a valence-band offset $\Lambda\approx360$ meV between CdTe and $Hg_{1-x}Zn_xTe$ ($x<0.1$) account perfectly for these data and show the existence of a semimetal-semiconductor transition which is induced by temperature. We have measured the cyclotron mass as a function of temperature with the magnetic field B applied both parallel and perpendicular to the SL growth axis. A strong mass anisotropy is observed in the semimetallic regime, while a rather low mass anisotropy (which can be less than unity) is measured in the semiconducting domain, as expected from the band-structure calculations. We have shown that the semimetal-semiconductor transition is characterized by an important reduction of the cyclotron mass measured when **B** is perpendicular to the SL growth axis, again in good agreement with the theoretical dispersion relations. The observed magneto-optical intraband transitions are in very satisfying agreement with the calculated Landau levels and the Fermi energy. Finally, we have shown that the temperature-dependent band structure of these type-III Hg-based SL's presents unique features quite different from those of III-V heterostructures.

ACKNOWLEDGMENTS

This work was partly supported by a joint research program Centre National de la Recherche Scientifique (CNRS)/National Science Foundation and by the NATO research Grant No. 9.13/890519. We wish to thank J. M. Berroir from the Ecole Normale Supérieure for contributing to this work. The Laboratoire de Physique de la Matière condensée de l'Ecole Normale Supérieure is associated to CNRS and to University Paris 6.

[1]N. F. Johnson, P. M. Hui, and H. Ehrenreich, Phys. Rev. Lett. **61**, 1993 (1988).

[2]J. R. Meyer, C. A. Hoffman, F. J. Bartoli, J. W. Han, J. W. Cook, Jr., J. F. Schetzina, X. Chu, J. P. Faurie, and J. N. Schulman, Phys. Rev. B **38**, 2204 (1988).

[3]J. M. Perez, R. J. Wagner, J. R. Meyer, J. W. Han, J. W. Cook, Jr., and J. F. Schetzina, Phys. Rev. Lett. **61**, 2261 (1988).

[4]J. M. Berroir, Y. Guldner, J. P. Vieren, M. Voos, X. Chu, and J. P. Faurie, Phys. Rev. Lett. **62**, 2024 (1989).

[5]C. A. Hoffman, J. R. Meyer, F. J. Bartoli, Y. Lansari, J. W. Cook, Jr., and J. F. Schetzina, Phys. Rev. B **40**, 3867 (1989).

[6]C. A. Hoffman, J. R. Meyer, F. J. Bartoli, J. W. Han, J. W. Cook, Jr., J. F. Schetzina, and J. N. Schulman, Phys. Rev. B **39**, 5208 (1989).

[7]J. R. Meyer, R. J. Wagner, F. J. Bartoli, C. A. Hoffman, M. Dobrowolska, T. Wojtowicz, J. K. Furdyna, and L. R. Ram-Mohan, Phys. Rev. B **42**, 9050 (1990).

[8]J. P. Faurie, M. Boukerche, S. Sivananthan, J. Reno, and C. Hsu, Superlatt. Microstruct. **1**, 237 (1985).

[9]X. Chu, S. Sivananthan, and J. P. Faurie, Superlatt. Microstruct. **4**, 173 (1988).

[10]J. Reno, R. Sporken, Y. J. Kim, C. Hsu, and J. P. Faurie, Appl. Phys. Lett. **51**, 1545 (1987).

[11]J. M. Berroir, Y. Guldner, J. P. Vieren, M. Voos, and J. P. Faurie, Phys. Rev. B **34**, 891 (1986).

[12]J. Reno, I. K. Sou, J. P. Faurie, J. M. Berroir, Y. Guldner, and J. P. Vieren, Appl. Phys. Lett. **49**, 106 (1986).

[13]J. M. Berroir, Y. Guldner, and M. Voos, IEEE J. Quantum Electron. **QE-22**, 1793 (1986).

[14]B. Toulouse, R. Granger, S. Rolland, and R. Triboulet, J. Phys. **48**, 247 (1987).

[15]M. H. Weiler, in *Semiconductors and Semimetals*, edited by R.

K. Willardson and A. C. Beer (Academic, New York, 1981), Vol. 16, p. 119.
[16]J. S. Blakemore, in *Semiconductor Statistics,* edited by H. K. Henisch (Pergamon, Oxford, 1962), Vol. 3, p. 103.
[17]M. Voos, J. Manasses, Y. Guldner, J. M. Berroir, J. P. Vieren, and J. P. Faurie, Superlatt. Microstruct. **8**, 167 (1990).
[18]Y. Guldner, G. S. Boebinger, J. P. Vieren, M. Voos, and J. P. Faurie, Phys. Rev. B **36**, 2958 (1987).
[19]C. A. Hoffman, J. R. Meyer, R. J. Wagner, F. J. Bartoli, X. Chu, J. P. Faurie, L. R. Ram-Mohan, and H. Xie, J. Vac. Sci. Technol. A **8**, 1200 (1990).
[20]N. W. Ashcroft and N. D. Mermin, *Solid State Physics* (Holt, Rinehart and Winston, New York, 1976), p. 233.
[21]T. Duffield, R. Bhat, M. Koza, F. DeRosa, D. M. Hwang, P. Grabbe, and S. J. Allen, Jr., Phys. Rev. Lett. **56**, 2724 (1986).